Supplementary Material for "Understanding Thermoelectric Properties from High-Throughput Calculations: Trends, Insights, and Comparisons with Experiment"

Wei Chen[1,8], Jan-Hendrik Pöhls[2], Geoffroy Hautier[3], Danny Broberg[4], Saurabh Bajaj[1,5], Umut Aydemir[5,9], Zachary M. Gibbs[5], Hong Zhu[6], Mark Asta[4], G. Jeffrey Snyder[5,9], Bryce Meredig[7], Mary Anne White[2], Kristin Persson[1,4], and Anubhav Jain[1, *]

[1.] Lawrence Berkeley National Laboratory, Berkeley, California 94720, USA.
[2.] Department of Physics and Atmospheric Science, Dalhousie University, Halifax, Nova Scotia B3H 4R2, Canada.
[3.] Institut de la matiére condense et des nanosciences (IMCN), European Theoretical Spectroscopy Facility (ETSF), Université Catholique de Louvain, Chemin des étoiles 8, bte L7.03.01, Louvain-la-Neuve 1348, Belgium.
[4.] Department of Materials Science and Engineering, University of California, Berkeley Berkeley, California 94720, USA.
[5.] Department of Applied Physics and Materials Science, California Institute of Technology, Pasadena, California 91125, USA.
[6.] University of Michigan – Shanghai Jiao Tong University Joint Institute, Shanghai Jiao Tong University, Shanghai 200240, China.
[7.] Citrine Informatics, Redwood City, CA 94063, USA.
[8.] Department of Mechanical, Materials and Aerospace Engineering, Illinois Institute of Technology, Chicago, IL 60616, USA
[9.] Department of Materials Science and Engineering, Northwestern University, 2220 Campus Drive, Evanston, IL, USA

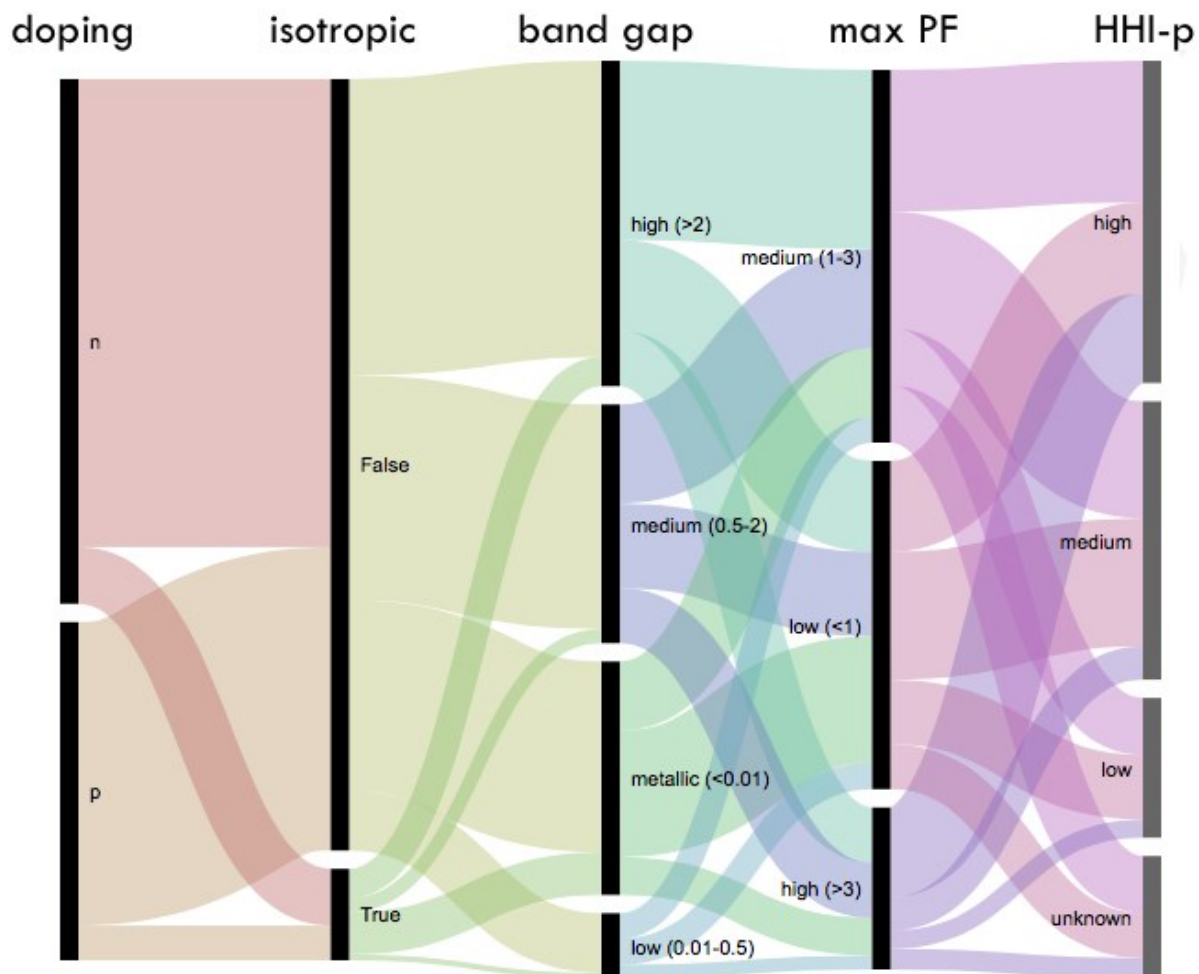* To whom correspondence should be addressed. Email: AJain@lbl.gov

Figure S1. Flow diagram representation of the data set of 48,770 compounds in this study. HHI-p column represents the Herfindahl−Hirschman Index of the elemental production data for the compounds. The other columns have the same meaning as in Figure 1.
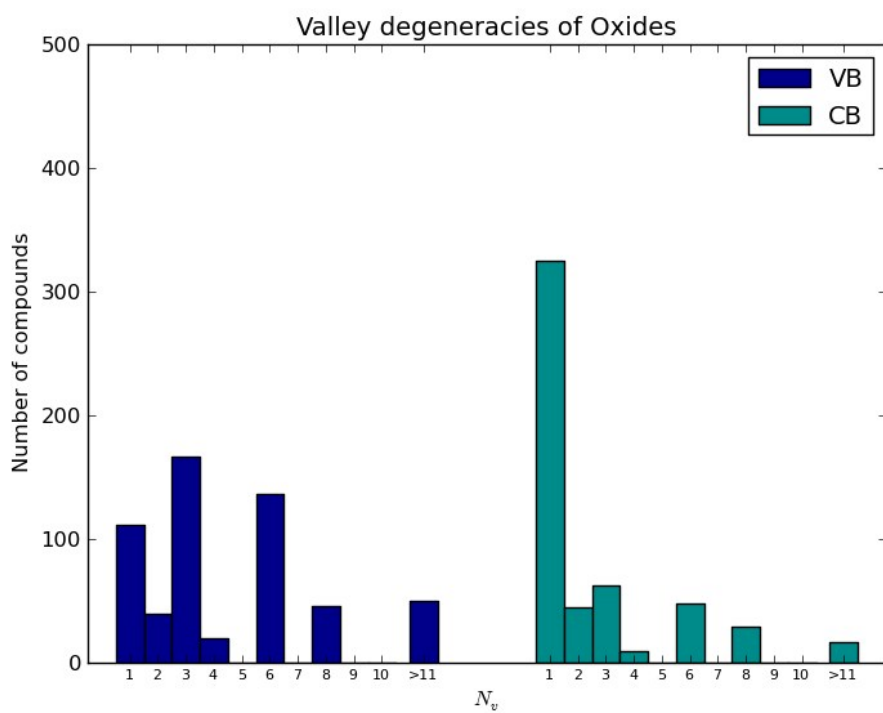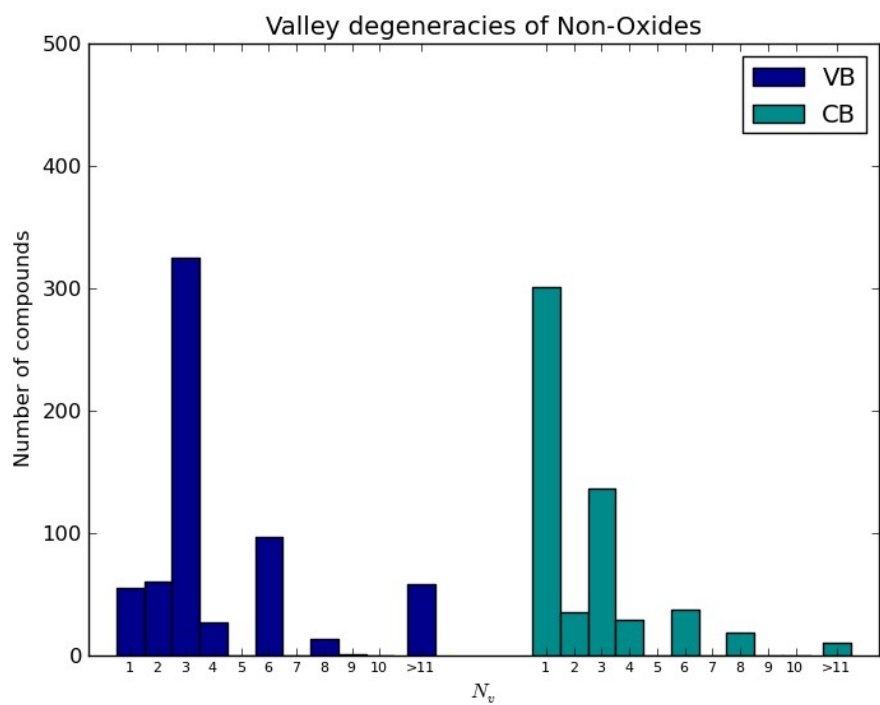
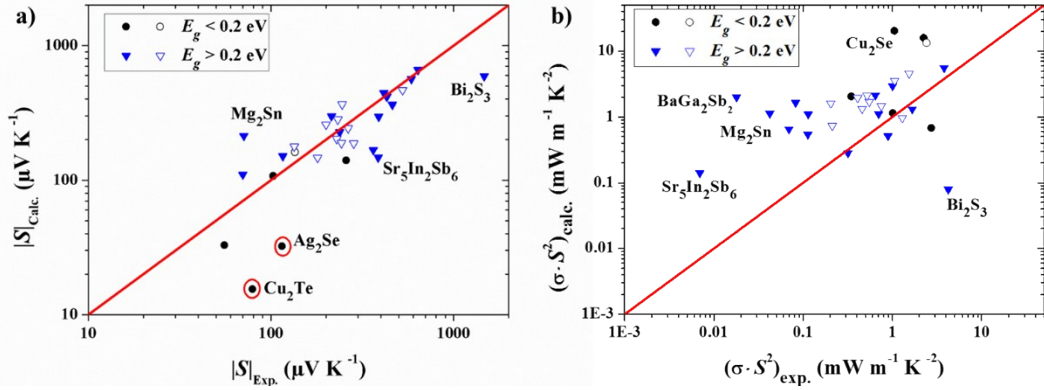Figure S2: Distribution of valley degeneracies of non-oxides and oxides.

Figure S3: Comparison of computed and experimental (a) Seebeck coefficients and (b) power factors for diverse thermoelectric materials (filled symbols) and the extrinsic doped compounds (hollow symbols). The band gap energies were scissored to the experimental band gap energy if the difference was larger than 50%. The red circles indicate that the sign of the Seebeck coefficient was incorrect (see Table S2). The red lines indicate equality of computation and experiment.

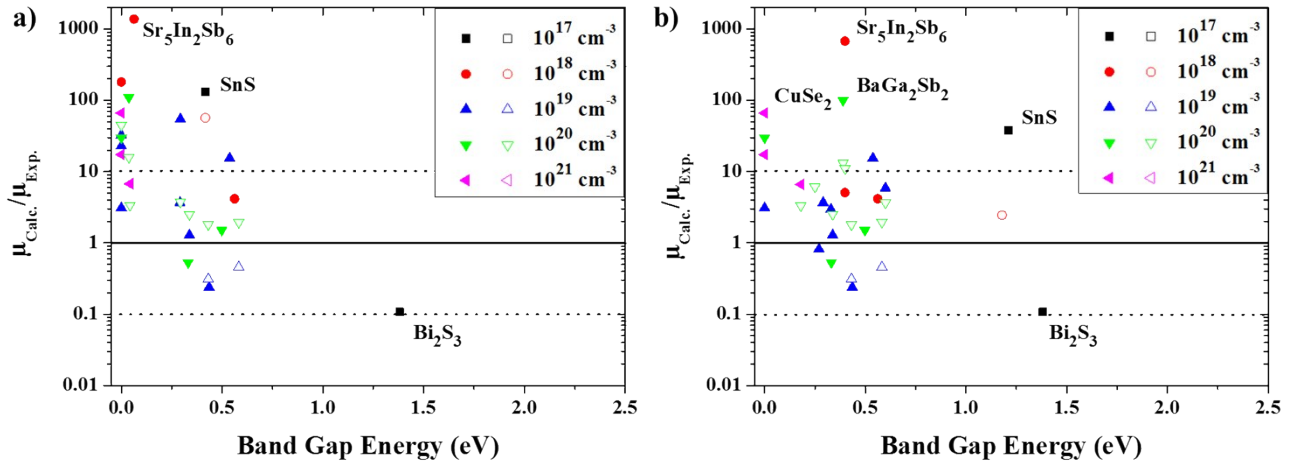Figure S4: The ratio of the calculated and experimental mobilities as a function of the calculated band gap energies for (a) the un-scissored computed data and (b) the scissored data. The hollow symbols denote extrinsically doped compounds. At low calculated band gaps, the mobility is vastly overestimated for most of the compounds. With increasing band gap energy, the computed mobilities agree more closely with experimental data.

4

Table S1: Calculated and experimental Seebeck coefficients (the temperature and Hall carrier concentrations at which the experimental Seebeck coefficients attained the maximum values were used) for different thermoelectric materials with DFT band gap energies. The plus sign in the Hall carrier concentration indicates *p*-type behavior and the minus sign indicates *n*-type behavior.

Material	Space Group No.	Temperature	Exp. Hall Carrier Conc.	Calc. Band Gap Energy	Exp. Seebeck	Calculated Seebeck	Ref.
		K	cm^{-3}	eV	$\mu V\ K^{-1}$	$\mu V\ K^{-1}$	
SnSe	63	923	+1.39E+19	0.29	388	295	[1]
SnSe	62	523	+3.16E+17	0.56	586	564	[1]
SnS	63	623	+1.79E+17	0.42	637	117	[2]
$SnS_{0.995}Ag_{0.05}$	63	627	+1.69E+18	0.42	525	196	[2]
SnTe	225	817	+1.00E+21	0.04	103	106	[3]
$Sn_{1.03}Te$	225	817	+3.49E+20	0.04	135	160	[3]
Cu_2Te	187	900	+2.00E+20	0.00	79.3	-15.5	[4]
Cu_2Se	216	900	+2.00E+21	0.00	258	140	[4]
Ag_2Se	17	310	-8.11E+18	0.00	-115	32.2	[5]
Bi_2S_3	62	480	-3.00E+17	1.38	-1470	-593	[6]
Bi_2Se_3	166	420	-2.20E+19	0.44	-70.0	-110	[7]
Bi_2Te_3	166	420	+7.78E+19	0.33	116	151	[8]
Sr_3GaSb_3	14	775	+8.05E+18	0.34	363	167	[9]
$Sr_3Ga_{0.93}Zn_{0.07}Sb_3$	14	980	+1.12E+20	0.34	229	202	[9]
ZrNiSn	216	600	-1.42E+20	0.50	-238	-227	[10]
Sr_3AlSb_3	64	825	+3.00E+19	0.54	462	363	[11]
Ca_3AlSb_3	62	690	+2.06E+18	0.29	414	71.1	[12]
$Ca_{2.94}Na_{0.06}AlSb_3$	62	1000	+7.17E+19	0.29	264	188	[12]
$SrZnSb_2$	62	600	+1.76E+21	0.00	55.6	32.8	[13]
$PbS_{0.9987}Cl_{0.0013}$	225	865	-2.45E+19	0.58	-232	-282	[14]
$PbS_{0.992}Cl_{0.008}$	225	865	-1.06E+20	0.58	-134	-178	[14]
$Na_{0.0025}Pb_{0.9975}Se$	225	750	+7.00E+18	0.43	245	365	[15]
$Na_{0.007}Pb_{0.993}Se$	225	824	+6.35E+19	0.43	200	258	[15]
$BaGa_2Sb_2$	62	360	+3.26E+18	0.04	431	56.1	[16]
$BaGa_{0.95}Zn_{0.05}Sb_2$	62	590	+7.73E+19	0.04	243	97.1	[16]
$Ca_5Ga_2Sb_6$	55	425	+4.31E+18	0.00	429	-38.6	[17]
$Ca_5Ga_{1.95}Zn_{0.05}Sb_6$	55	640	+1.72E+20	0.00	180	31.2	[17]
Mg_2Sn	225	400	-2.00E+19	0.00	-71.5	22.4	[18]
$Sr_5In_2Sb_6$	55	475	+5.98E+17	0.06	386	-70.9	[19]
$Sr_5In_{1.9}Zn_{0.1}Sb_6$	55	700	+1.19E+20	0.06	284	80.9	[19]
$SrZn_2Sb_2$	164	600	+1.63E+19	0.00	214	40.6	[20]

Table S2: Calculated and experimental Seebeck coefficients (the temperature and carrier concentrations at which the experimental Seebeck coefficients attained the maximum values were used) for different thermoelectric materials with scissored band gap energies (underlined). The plus sign in the Hall carrier concentration indicates *p*-type behavior and the minus sign indicates *n*-type behavior.

Material	Space Group No.	Temperature	Exp. Hall Carrier Conc.	Calc. Band Gap Energy	Exp. Seebeck	Calculated Seebeck	Ref.
		K	cm^{-3}	eV	μV K^{-1}	μV K^{-1}	
SnSe	63	923	+1.39E+19	0.29	388	295	[1]
SnSe	62	523	+3.16E+17	0.56	586	564	[1]
SnS	63	623	+1.79E+17	1.21	637	658	[2]
SnS$_{0.995}$Ag$_{0.05}$	63	627	+1.69E+18	1.18	525	466	[2]
SnTe	225	817	+1.00E+21	0.18	103	107	[3]
Sn$_{1.03}$Te	225	817	+3.49E+20	0.18	135	161	[3]
Cu$_2$Te	187	900	+2.00E+20	0.00	79.3	-15.5	[4]
Cu$_2$Se	216	900	+2.00E+21	0.00	258	140	[4]
Ag$_2$Se	17	310	-8.11E+18	0.00	-115	32.2	[5]
Bi$_2$S$_3$	62	480	-3.00E+17	1.38	-1470	-593	[6]
Bi$_2$Se$_3$	166	420	-2.20E+19	0.44	-70.0	-110	[7]
Bi$_2$Te$_3$	166	420	+7.78E+19	0.33	116	151	[8]
Sr$_3$GaSb$_3$	14	775	+8.05E+18	0.34	363	167	[9]
Sr$_3$Ga$_{0.93}$Zn$_{0.07}$Sb$_3$	14	980	+1.12E+20	0.34	229	202	[9]
ZrNiSn	216	600	-1.42E+20	0.50	-238	-227	[10]
Sr$_3$AlSb$_3$	64	825	+3.00E+19	0.54	462	363	[11]
Ca$_3$AlSb$_3$	62	690	+2.06E+18	0.60	414	444	[12]
Ca$_{2.94}$Na$_{0.06}$AlSb$_3$	62	1000	+7.17E+19	0.60	264	243	[12]
SrZnSb$_2$	62	600	+1.76E+21	0.00	55.6	32.8	[13]
PbS$_{0.9987}$Cl$_{0.0013}$	225	865	-2.45E+19	0.58	-232	-282	[14]
PbS$_{0.992}$Cl$_{0.008}$	225	865	-1.06E+20	0.58	-134	-178	[14]
Na$_{0.0025}$Pb$_{0.9975}$Se	225	750	+7.00E+18	0.43	245	365	[15]
Na$_{0.007}$Pb$_{0.993}$Se	225	824	+6.35E+19	0.43	200	258	[15]
BaGa$_2$Sb$_2$	62	360	+3.26E+18	0.39	431	417	[16]
BaGa$_{0.95}$Zn$_{0.05}$Sb$_2$	62	590	+7.73E+19	0.39	243	188	[16]
Ca$_5$Ga$_2$Sb$_6$	55	425	+4.31E+18	0.40	429	418	[17]
Ca$_5$Ga$_{1.95}$Zn$_{0.05}$Sb$_6$	55	640	+1.72E+20	0.25	180	147	[17]
Mg$_2$Sn	225	400	-2.00E+19	0.33	-71.5	-213	[18]
Sr$_5$In$_2$Sb$_6$	55	475	+5.98E+17	0.40	386	147	[19]
Sr$_5$In$_{1.9}$Zn$_{0.1}$Sb$_6$	55	700	+1.19E+20	0.40	284	187	[19]
SrZn$_2$Sb$_2$	164	600	+1.63E+19	0.27	214	298	[20]

Table S3: Calculated and experimental power factors (the temperature and carrier concentrations at which the experimental power factors attained the maximum values were used) for different thermoelectric materials with DFT band gap energies. The plus sign in the Hall carrier concentration indicates *p*-type behavior and the minus sign indicates *n*-type behavior.

Material	Space Group No.	Temperature	Exp. Hall Carrier Conc.	Calc. Band Gap Energy	Exp. Power Factor	Calculated Power Factor	Ref.
		K	cm^{-3}	eV	mW m^{-1} K^{-2}	mW m^{-1} K^{-2}	
SnSe	63	823	+1.18E+19	0.29	1.00	2.95	[1]
SnSe	62	773	+7.21E+18	0.56	0.64	2.14	[1]
SnS	63	823	+9.34E+18	0.42	0.08	1.52	[2]
SnS$_{0.995}$Ag$_{0.05}$	63	823	+2.40E+18	0.42	0.21	1.00	[2]
SnTe	225	817	+1.00E+21	0.04	2.24	15.64	[3]
Sn$_{1.03}$Te	225	768	+3.10E+20	0.04	2.40	13.14	[3]
Cu$_2$Te	187	900	+2.00E+20	0.00	1.01	1.14	[4]
Cu$_2$Se	216	900	+2.00E+21	0.00	1.05	20.34	[4]
Ag$_2$Se	17	330	-8.77E+18	0.00	2.73	0.68	[5]
Bi$_2$S$_3$	62	450	-3.00E+17	1.38	4.22	0.08	[6]
Bi$_2$Se$_3$	166	420	-2.20E+19	0.44	0.89	0.51	[7]
Bi$_2$Te$_3$	166	350	+6.92E+19	0.33	1.66	1.31	[8]
Sr$_3$GaSb$_3$	14	600	+5.50E+18	0.34	0.32	0.28	[9]
Sr$_3$Ga$_{0.93}$Zn$_{0.07}$Sb$_3$	14	980	+1.12E+20	0.34	0.75	1.46	[9]
ZrNiSn	216	870	-2.66E+20	0.50	3.80	5.54	[10]
Sr$_3$AlSb$_3$	64	840	+3.50E+19	0.54	0.11	1.10	[11]
Ca$_3$AlSb$_3$	62	1034	+1.66E+19	0.29	0.07	0.36	[12]
Ca$_{2.94}$Na$_{0.06}$AlSb$_3$	62	1020	+7.76E+19	0.29	0.55	1.06	[12]
SrZnSb$_2$	62	600	+1.76E+21	0.00	0.34	2.06	[13]
PbS$_{0.9987}$Cl$_{0.0013}$	225	500	-2.36E+19	0.58	0.46	1.33	[14]
PbS$_{0.992}$Cl$_{0.008}$	225	865	-1.06E+20	0.58	1.06	3.58	[14]
Na$_{0.0025}$Pb$_{0.9975}$Se	225	500	+8.63E+18	0.43	1.29	0.96	[15]
Na$_{0.007}$Pb$_{0.993}$Se	225	824	+6.35E+19	0.43	1.54	4.56	[15]
BaGa$_2$Sb$_2$	62	820	+1.58E+20	0.04	0.02	0.65	[16]
BaGa$_{0.95}$Zn$_{0.05}$Sb$_2$	62	590	+7.73E+19	0.04	0.20	0.53	[16]
Ca$_5$Ga$_2$Sb$_6$	55	425	+4.31E+18	0.00	0.11	0.16	[17]
Ca$_5$Ga$_{1.95}$Zn$_{0.05}$Sb$_6$	55	640	+1.72E+20	0.00	0.52	0.70	[17]
Mg$_2$Sn	225	400	-2.00E+19	0.00	0.04	0.14	[18]
Sr$_5$In$_2$Sb$_6$	55	600	+1.75E+18	0.06	0.01	0.37	[19]
Sr$_5$In$_{1.9}$Zn$_{0.1}$Sb$_6$	55	700	+1.19E+20	0.06	0.41	1.18	[19]
SrZn$_2$Sb$_2$	164	600	+1.63E+19	0.00	0.70	0.57	[20]

Table S4: Calculated and experimental power factors (the temperature and carrier concentrations at which the experimental power factors attained the maximum values were used) for different thermoelectric materials with scissored band gap energies (underlined). The plus sign in the Hall carrier concentration indicates *p*-type behavior and the minus sign indicates *n*-type behavior.

Material	Space Group No.	Temperature	Exp. Hall Carrier Conc.	Calc. Band Gap Energy	Exp. Power Factor	Calculated Power Factor	Ref.
		K	cm^{-3}	eV	mW m^{-1} K^{-2}	mW m^{-1} K^{-2}	
SnSe	63	823	+1.18E+19	0.29	1.00	2.95	[1]
SnSe	62	773	+7.21E+18	0.56	0.64	2.14	[1]
SnS	63	823	+9.34E+18	1.21	0.08	1.65	[2]
SnS$_{0.995}$Ag$_{0.05}$	63	823	+2.40E+18	1.18	0.21	0.73	[2]
SnTe	225	817	+1.00E+21	0.18	2.24	15.9	[3]
Sn$_{1.03}$Te	225	768	+3.10E+20	0.18	2.40	13.3	[3]
Cu$_2$Te	187	900	+2.00E+20	0.00	1.01	1.14	[4]
Cu$_2$Se	216	900	+2.00E+21	0.00	1.05	20.34	[4]
Ag$_2$Se	17	330	-8.77E+18	0.00	2.73	0.68	[5]
Bi$_2$S$_3$	62	450	-3.00E+17	1.38	4.22	0.08	[6]
Bi$_2$Se$_3$	166	420	-2.20E+19	0.44	0.89	0.51	[7]
Bi$_2$Te$_3$	166	350	+6.92E+19	0.33	1.66	1.31	[8]
Sr$_3$GaSb$_3$	14	600	+5.50E+18	0.34	0.32	0.28	[9]
Sr$_3$Ga$_{0.93}$Zn$_{0.07}$Sb$_3$	14	980	+1.12E+20	0.34	0.75	1.46	[9]
ZrNiSn	216	870	-2.66E+20	0.50	3.80	5.54	[10]
Sr$_3$AlSb$_3$	64	840	+3.50E+19	0.54	0.11	1.10	[11]
Ca$_3$AlSb$_3$	62	1034	+1.66E+19	0.60	0.07	0.65	[12]
Ca$_{2.94}$Na$_{0.06}$AlSb$_3$	62	1020	+7.76E+19	0.60	0.55	1.69	[12]
SrZnSb$_2$	62	600	+1.76E+21	0.00	0.34	2.06	[13]
PbS$_{0.9987}$Cl$_{0.0013}$	225	500	-2.36E+19	0.58	0.46	1.33	[14]
PbS$_{0.992}$Cl$_{0.008}$	225	865	-1.06E+20	0.58	1.06	3.58	[14]
Na$_{0.0025}$Pb$_{0.9975}$Se	225	500	+8.63E+18	0.43	1.29	0.96	[15]
Na$_{0.007}$Pb$_{0.993}$Se	225	824	+6.35E+19	0.43	1.54	4.56	[15]
BaGa$_2$Sb$_2$	62	820	+1.58E+20	0.39	0.02	1.99	[16]
BaGa$_{0.95}$Zn$_{0.05}$Sb$_2$	62	590	+7.73E+19	0.39	0.20	1.61	[16]
Ca$_5$Ga$_2$Sb$_6$	55	425	+4.31E+18	0.40	0.11	0.54	[17]
Ca$_5$Ga$_{1.95}$Zn$_{0.05}$Sb$_6$	55	640	+1.72E+20	0.25	0.52	2.11	[17]
Mg$_2$Sn	225	400	-2.00E+19	0.33	0.04	1.13	[18]
Sr$_5$In$_2$Sb$_6$	55	600	+1.75E+18	0.40	0.01	0.14	[19]
Sr$_5$In$_{1.9}$Zn$_{0.1}$Sb$_6$	55	700	+1.19E+20	0.40	0.41	1.94	[19]
SrZn$_2$Sb$_2$	164	600	+1.63E+19	0.27	0.70	1.11	[20]

Table S5: Calculated and experimental mobilities for different thermoelectric materials with DFT band gap energies. *p*-type indicates that it is the hole mobility and *n*-type indicates that it is the electron mobility.

Material	Space Group No.	Type	Band Gap Calc. eV	Mobility Exp. $cm^2\ V^{-1}\ s^{-1}$	Mobility Calc. $cm^2\ V^{-1}\ s^{-1}$	Ratio Mobilities (Calc./Exp.)	Ref.
SnSe	63	*p*	0.29	45	165	3.68	[1]
SnSe	62	*p*	0.56	29	121	4.14	[1]
SnS	63	*p*	0.42	2.11	278	56.2	[2]
$SnS_{0.995}Ag_{0.05}$	63	*p*	0.42	33	1854	2.45	[2]
SnTe	225	*p*	0.04	13	88	6.77	[3]
$Sn_{1.03}Te$	225	*p*	0.04	31	106	3.42	[3]
Cu_2Te	187	*p*	0.00	50	1486	29.7	[4]
Cu_2Se	216	*p*	0.00	0.49	32	66.5	[4]
Ag_2Se	17	*n*	0.00	1564	4853	3.10	[5]
Bi_2S_3	62	*n*	1.38	454	49	0.11	[6]
Bi_2Se_3	166	*n*	0.44	516	123	0.24	[7]
Bi_2Te_3	166	*p*	0.33	125	66	0.53	[8]
Sr_3GaSb_3	14	*p*	0.34	28	36	1.28	[9]
$Sr_3Ga_{0.93}Zn_{0.07}Sb_3$	14	*p*	0.34	7.97	20	2.51	[9]
ZrNiSn	216	*n*	0.50	18	27	1.50	[10]
Sr_3AlSb_3	64	*p*	0.54	1.02	16	15.5	[11]
Ca_3AlSb_3	62	*p*	0.29	4.37	240	54.9	[12]
$Ca_{2.94}Na_{0.06}AlSb_3$	62	*p*	0.29	6.52	24	3.68	[12]
$SrZnSb_2$	62	*p*	0.00	3.94	68	17.3	[13]
$PbS_{0.9987}Cl_{0.0013}$	225	*n*	0.58	170	78	0.46	[14]
$PbS_{0.992}Cl_{0.008}$	225	*n*	0.58	35	68	1.95	[14]
$Na_{0.0025}Pb_{0.9975}Sb$	225	*p*	0.43	295	92	0.31	[15]
$Na_{0.007}Pb_{0.993}Sb$	225	*p*	0.43	38	67	1.79	[15]
$BaGa_2Sb_2$	62	*p*	0.04	0.31	35	112	[16]
$BaGa_{0.95}Zn_{0.05}Sb_2$	62	*p*	0.04	2.78	44	15.8	[16]
$Ca_5Ga_2Sb_6$	55	*p*	0.00	8.88	1605	182	[17]
$Ca_5Ga_{1.95}Zn_{0.05}Sb_6$	55	*p*	0.00	5.82	260	6.12	[17]
Mg_2Sn	225	*n*	0.00	26	853	44.7	[18]
$Sr_5In_2Sb_6$	55	*p*	0.06	2.34	3234	1381	[19]
$Sr_5In_{1.9}Zn_{0.1}Sb_6$	55	*p*	0.06	2.63	94	35.7	[19]
$SrZn_2Sb_2$	164	*p*	0.00	59	1339	22.7	[20]

9

Table S6: Calculated and experimental mobilities for different thermoelectric materials with scissored band gap energies (underlined). *p*-type indicates that it is the hole mobility and *n*-type indicates that it is the electron mobility.

Material	Space Group No.	Type	Band Gap Calc. eV	Mobility Exp. $cm^2\ V^{-1}\ s^{-1}$	Mobility Calc. $cm^2\ V^{-1}\ s^{-1}$	Ratio Mobilities (Calc./Exp.)	Ref.
SnSe	63	*p*	0.29	45	165	3.68	[1]
SnSe	62	*p*	0.56	29	121	4.14	[1]
SnS	63	*p*	1.21	2.11	80	37.7	[2]
$SnS_{0.995}Ag_{0.05}$	63	*p*	1.18	33	80	2.45	[2]
SnTe	225	*p*	0.18	13	86	6.61	[3]
$Sn_{1.03}Te$	225	*p*	0.18	31	105	3.33	[3]
Cu_2Te	187	*p*	0.00	50	1486	29.7	[4]
Cu_2Se	216	*p*	0.00	0.49	32	66.5	[4]
Ag_2Se	17	*n*	0.00	1564	4853	3.10	[5]
Bi_2S_3	62	*n*	1.38	454	49	0.11	[6]
Bi_2Se_3	166	*n*	0.44	516	123	0.24	[7]
Bi_2Te_3	166	*p*	0.33	125	66	0.53	[8]
Sr_3GaSb_3	14	*p*	0.34	28	36	1.28	[9]
$Sr_3Ga_{0.93}Zn_{0.07}Sb_3$	14	*p*	0.34	7.97	20	2.51	[9]
ZrNiSn	216	*n*	0.50	18	27	1.50	[10]
Sr_3AlSb_3	64	*p*	0.54	1.02	16	15.5	[11]
Ca_3AlSb_3	62	*p*	0.60	4.37	26	5.89	[12]
$Ca_{2.94}Na_{0.06}AlSb_3$	62	*p*	0.60	6.52	24	3.64	[12]
$SrZnSb_2$	62	*p*	0.00	3.94	68	17.3	[13]
$PbS_{0.9987}Cl_{0.0013}$	225	*n*	0.58	170	78	0.46	[14]
$PbS_{0.992}Cl_{0.008}$	225	*n*	0.58	35	68	1.95	[14]
$Na_{0.0025}Pb_{0.9975}Sb$	225	*p*	0.43	295	92	0.31	[15]
$Na_{0.007}Pb_{0.993}Sb$	225	*p*	0.43	38	67	1.79	[15]
$BaGa_2Sb_2$	62	*p*	0.39	0.31	31	99.6	[16]
$BaGa_{0.95}Zn_{0.05}Sb_2$	62	*p*	0.39	2.78	37	13.2	[16]
$Ca_5Ga_2Sb_6$	55	*p*	0.40	8.88	45	5.06	[17]
$Ca_5Ga_{1.95}Zn_{0.05}Sb_6$	55	*p*	0.25	5.82	36	6.12	[17]
Mg_2Sn	225	*n*	0.33	26	78	2.97	[18]
$Sr_5In_2Sb_6$	55	*p*	0.40	2.34	1581	675	[19]
$Sr_5In_{1.9}Zn_{0.1}Sb_6$	55	*p*	0.40	2.63	29	11.0	[19]
$SrZn_2Sb_2$	164	*p*	0.27	59	48	0.82	[20]

Table S7: Experimental minimum thermal conductivities compared to thermal conductivities calculated using the Clarke and the Cahill-Pohl models.

Formula	κmin Exp. W m-1 K-1	κClarke W m-1 K-1	κCahill W m-1 K-1	Reference
AgBr	0.43	0.29	0.35	[21]
Bi_2Te_3	0.58	0.21	0.23	[22]
$NaCo_2O_4$	0.71	1.00	1.12	[23]
KBr	0.67	0.29	0.33	[24]
$BaTiO_3$	2.38	1.44	1.56	[25]
Mg_2Si	2.64	1.13	1.22	[26]
TiO_2	3.30	1.52	1.73	[27]
SiO_2	1.24	1.09	1.19	[23]
$SrTiO_3$	1.73	1.67	1.81	[28]
Y_2O_3	2.95	1.11	1.23	[29]
$MgAl_2O_4$	5.47	2.21	2.41	[30]
GaAs	3.20	0.65	0.70	[31]
MgO	6.02	2.39	2.58	[30]
ZnO	1.72	1.01	1.17	[30]
Ge	0.51	0.67	0.72	[24]
Si_3N_4	2.00	2.46	2.70	[30]
Si	1.05	1.29	1.39	[30]
GaN	6.00	1.83	1.98	[30]
BeO	15.00	3.69	3.98	[32]
NiO	1.92	1.65	1.80	[33]
$AgCrSe_2$	0.15	0.49	0.56	[34]
WO_3	1.52	1.39	1.52	[30]
Mo_6Te_8	1.10	0.30	0.34	[35]
ZrO_2	2.50	1.42	1.57	[32]
Co_4Sb	0.40	0.63	0.68	[36]

Note: Data used to generate the cluster labels for generating Figures 8 and 9 are available in a secondary supporting document entitled Suppl_material_clusterlabels.xlsx .

References

1   L.-D. Zhao, S.-H. Lo, Y. Zhang, H. Sun, G. Tan, C. Uher, C. Wolverton, V. P. Dravid and M. G. Kanatzidis, *Nature*, 2014, **508**, 373–377.

2   Q. Tan, L.-D. Zhao, J.-F. Li, C.-F. Wu, T.-R. Wei, Z.-B. Xing and M. G. Kanatzidis, *J. Mater. Chem. A*, 2014, **2**, 17302–17306.

3   G. Tan, L. D. Zhao, F. Shi, J. W. Doak, S. H. Lo, H. Sun, C. Wolverton, V. P. Dravid, C. Uher and M. G. Kanatzidis, *J. Am. Chem. Soc.*, 2014, **136**, 7006–7017.

4   S. Ballikaya, H. Chi, J. R. Salvador and C. Uher, *J. Mater. Chem. A*, 2013, **1**, 12478–12484.

5   W. Mi, P. Qiu, T. Zhang, Y. Lv, X. Shi and L. Chen, *Appl. Phys. Lett.*, 2014, **104**, 133903.

6   S. C. Liufu, L. D. Chen, Q. Yao and C. F. Wang, *Appl. Phys. Lett.*, 2007, **90**, 112106.

7   P. Janíček, Č. Drašar, L. Beneš and P. Lošták, *Cryst. Res. Technol.*, 2009, **44**, 505–510.

8   Y. Zhang, H. Wang, S. Kräemer, Y. Shi, F. Zhang, M. Snedaker, K. Ding, M. Moskovits, G. J. Snyder and G. D. Stucky, *ACS Nano*, 2011, **5**, 3158–3165.

9   A. Zevalkink, W. G. Zeier, G. Pomrehn, E. Schechtel, W. Tremel and G. J. Snyder, *Energy Environ. Sci.*, 2012, **5**, 9121–9128.

10 H. Xie, H. Wang, C. Fu, Y. Liu, G. J. Snyder, X. Zhao and T. Zhu, *Sci. Rep.*, 2014, **4**, 6888.

11 A. Zevalkink, G. Pomrehn, Y. Takagiwa, J. Swallow and G. J. Snyder, *ChemSusChem*, 2013, **6**, 2316–2321.

12 A. Zevalkink, E. S. Toberer, W. G. Zeier, E. Flage-Larsen and G. J. Snyder, *Energy Environ. Sci.*, 2011, **4**, 510–518.

13 A. F. May, E. S. Toberer and G. J. Snyder, *J. Appl. Phys.*, 2009, **106**, 013706.

14 H. Wang, E. Schechtel, Y. Pei and G. J. Snyder, *Adv. Energy Mater.*, 2013, **3**, 488–495.

15 H. Wang, Y. Pei, A. D. Lalonde and G. J. Snyder, *Adv. Mater.*, 2011, **23**, 1366–1370.

16 U. Aydemir, A. Zevalkink, A. Ormeci, Z. M. Gibbs, S. Bux and G. J. Snyder, *Chem. Mater.*, 2015, **27**, 1622–1630.

17 S. I. Johnson, A. Zevalkink and G. J. Snyder, *J. Mater. Chem. A*, 2013, **1**, 4244.

18 S. Kim, B. Wiendlocha, H. Jin, J. Tobola and J. P. Heremans, *J. Appl. Phys.*, 2014, **116**, 153706.

19 S. Chanakian, A. Zevalkink, U. Aydemir, Z. M. Gibbs, G. Pomrehn, J.-P. Fleurial, S. Bux and G. J. Snyder, *J. Mater. Chem. A*, 2015, **3**, 10289–10295.

20 E. S. Toberer, A. F. May, B. C. Melot, E. Flage-Larsen and G. J. Snyder, *Dalt. Trans.*, 2010, **39**, 1046–1054.

21 T. E. Pochapsky, *J. Chem. Phys.*, 1953, **21**, 1539.

22   Y. Zhao, J. S. Dyck and C. Burda, *J. Mater. Chem.*, 2011, **21**, 17049–17058.

23   T. M. Tritt, *Thermal conductivity: theory, properties, and applications*, Springer Science & Business Media, 2004.

24   D. Cahill, S. Watson and R. Pohl, *Phys. Rev. B*, 1992, **46**.

25   H. Muta, K. Kurosaki and S. Yamanaka, *J. Alloys Compd.*, 2004, **368**, 22–24.

26   K. Mars, H. Ihou-Mouko, G. Pont, J. Tobola and H. Scherrer, *J. Electron. Mater.*, 2009, **38**, 1360–1364.

27   S.-M. Lee, D. G. Cahill and T. H. Allen, *Phys. Rev. B*, 1995, **52**, 253.

28   D. W. Oh, J. Ravichandran, C. W. Liang, W. Siemons, B. Jalan, C. M. Brooks, M. Huijben, D. G. Schlom, S. Stemmer, L. W. Martin, A. Majumdar, R. Ramesh and D. G. Cahill, *Appl. Phys. Lett.*, 2011, **98**, 221904.

29   W. J. Tropf, M. E. Thomas and T. J. Harris, *Handb. Opt.*, 1995, **2**, 33–61.

30   S. Shindé and J. Goela, *High thermal conductivity materials*, 2006.

31   T. Borca-Tasciuc, D. W. Song, J. R. Meyer, I. Vurgaftman, M. J. Yang, B. Z. Nosho, L. J. Whitman, H. Lee, R. U. Martinelli and G. W. Turner, *Thermal Conductivity of AlAs (0.07) Sb (0.93) and Al (0.9) Ga (0.1) As (0.07) Sb (0.93) Alloys and (AlAs) 1/(AlSB) 11 Digital-Alloy Superlattices*, DTIC Document, 2002.

32   C. G. Levi, *Curr. Opin. Solid State Mater. Sci.*, 2004, **8**, 77–91.

33   W. Shin and N. Murayama, *Jpn. J. Appl. Phys.*, 1999, **38**, L1336.

34   F. Gascoin and A. Maignan, *Chem. Mater.*, 2011, **23**, 2510–2513.

35   K. Kurosaki, A. Kosuga and S. Yamanaka, 2003, **351**, 208–211.

36   K. Biswas, M. S. Good, K. C. Roberts, M. A. Subramanian and T. J. Hendricks, *J. Mater. Res.*, 2011, **26**, 1827–1835.